Electrochemistry Communications 49 (2014) 51–54

Contents lists available at ScienceDirect

Electrochemistry Communications

journal homepage: www.elsevier.com/locate/elecom

Short communication

O3-type $Na(Mn_{0.25}Fe_{0.25}Co_{0.25}Ni_{0.25})O_2$: A quaternary layered cathode compound for rechargeable Na ion batteries

Xin Li [a], Di Wu [b], Yong-Ning Zhou [c], Lei Liu [a], Xiao-Qing Yang [c], Gerbrand Ceder [a,*]

[a] Department of Materials Science and Engineering, Massachusetts Institute of Technology, MA 02139, USA
[b] Department of Mechanical Engineering, Massachusetts Institute of Technology, MA 02139, USA
[c] Chemistry Department, Brookhaven National Laboratory, Upton, NY 11973, USA

ARTICLE INFO

Article history:
Received 23 September 2014
Received in revised form 5 October 2014
Accepted 5 October 2014
Available online 13 October 2014

Keywords:
$Na(Mn_{0.25}Fe_{0.25}Co_{0.25}Ni_{0.25})O_2$
Quaternary
$Na(Ni_{0.5}Mn_{0.5})O_2$
$Na(Fe_{0.5}Co_{0.5})O_2$
Sodium
Na-ion battery

ABSTRACT

We report a new layered $Na(Mn_{0.25}Fe_{0.25}Co_{0.25}Ni_{0.25})O_2$ compound with O3 oxygen stacking. It delivers 180 mAh/g initial discharge capacity and 578 Wh/kg specific energy density with good cycling capability at high cutoff voltage. In situ X-ray diffraction (XRD) shows a reversible structure evolution of O3-P3-O3′-O3″ upon Na de-intercalation. The excellent capacity and cycling performance at high cutoff voltage make it an important model system for studying the general issue of capacity fading in layered Na cathode compounds.

1. Introduction

Layered sodium metal oxides have attracted considerable interest as cathodes for Na-ion batteries partly due to the fact that all seven layered $NaTMO_2$ with the O3-structure, where TM is a single oxidizable 3d transition metal ion from Ti, V, Cr, Mn, Fe, Co, Ni [1], can be easily synthesized, and show the capability to intercalate Na ions reversibly [2–7]. This is very different from their Li analogues, where only $LiCoO_2$ and $LiNiO_2$ reversibly intercalate Li ions [8]. Furthermore, different transition metal ions can be easily mixed in the TM layer to make new $NaTMO_2$ compounds [9–15]. Among them, O3-$Na(Fe_{0.5}Co_{0.5})O_2$ (denoted hereafter as FC) shows a capacity around 160 mAh/g with excellent capacity retention when cycled below 4.0 V and an average voltage of 3.14 V [11]. O3-$Na(Ni_{0.5}Mn_{0.5})O_2$ (denoted hereafter as NM) shows an initial discharge capacity of 185 mAh/g and average voltage of 3.22 V, partly due to a long high voltage plateau around 4.0 V [12,16]. But capacity retention of NM is poor if the 4.0 V plateau is included in the galvanostatic cycling.

We report here in this communication a new quaternary O3-structured compound with composition $Na(Mn_{0.25}Fe_{0.25}Co_{0.25}Ni_{0.25})O_2$ (denoted hereafter as MFCN), with theoretical capacity of 239 mAh/g and initial discharge capacity of 180 mAh/g over an average discharge voltage of 3.21 V. More importantly, its capacity retention is significantly improved over NM and FC even when cycled with high charge voltage cutoff. In-situ lab X-ray diffraction (XRD) to reveal the structure evolution of MFCN in the first electrochemical cycle shows a reversible O3-P3-O3′-O3″ phase transformation. Our result shows the opportunity to further improve the electrochemical performance of layered $NaTMO_2$ compounds by designing new combinations of transition metal ions in the TM layer.

2. Experimental

Stoichiometric amounts of Na_2CO_3 (99.95% Alfa Aesar), Mn_2O_3 (99.99% Sigma-Aldrich), Fe_2O_3 (99.99% Alfa Aesar), Co_3O_4 (99.7% Alfa Aesar), and NiO (99.99% Sigma-Aldrich) powder were mixed and pressed into a pellet. MFCN was synthesized by sintering the pellet at 900 °C in an oxygen gas flow for 12 h. The pellet was quenched to room temperature and transferred immediately into an Ar-filled glovebox. An XRD sample was sealed with Kapton film inside the glovebox and then scanned from 10° to 85° 2θ angle on a PANalytical X'pert PRO diffractometer equipped with a Cu Kα radiation source. Structure analysis using the Rietveld method was carried out using Highscore Plus.

The X-ray absorption spectroscopy (XAS) at the Mn, Fe, Co and Ni K-edge were collected in a transmission mode at beamline X18A of the National Synchrotron Light Source (NSLS) at Brookhaven National Laboratory. Energy calibration was carried out using the first inflection point of the reference spectrum of Mn, Fe, Co and Ni-metallic foils

* Corresponding author.
E-mail address: gceder@mit.edu (G. Ceder).

http://dx.doi.org/10.1016/j.elecom.2014.10.003

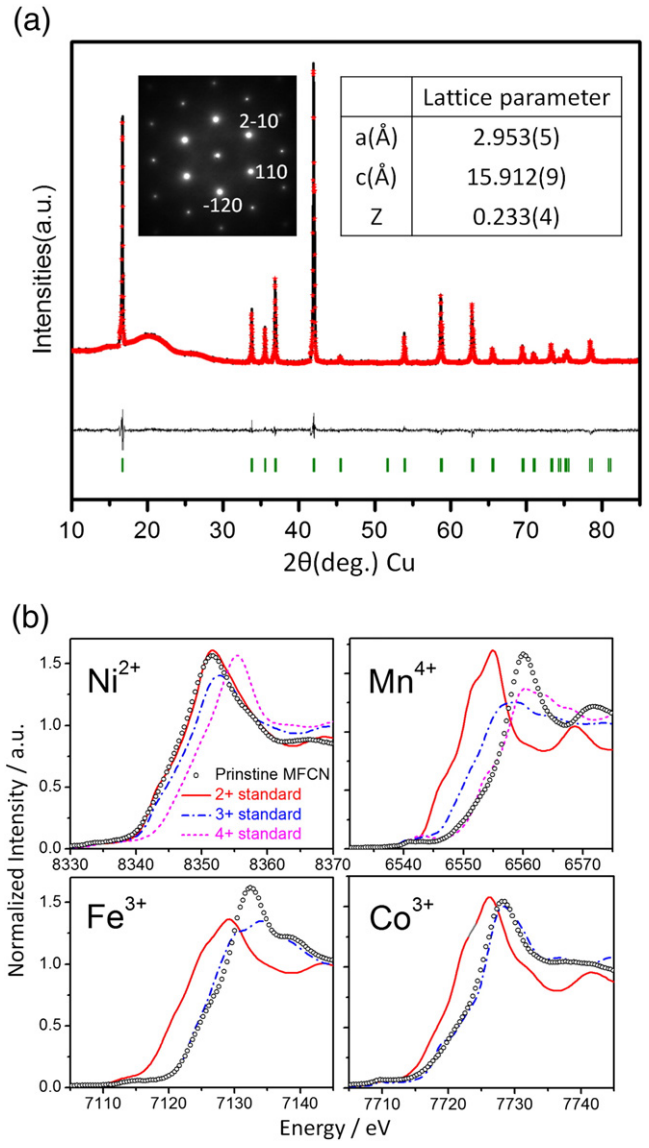

Fig. 1. (a) The powder XRD refinement of O3-Na($Mn_{0.25}Fe_{0.25}Co_{0.25}Ni_{0.25}$)$O_2$ (MFCN) using R-3 m symmetry. The goodness of fit is 4.35 and Rwp is 2.18. The inset table shows the refined lattice parameters. The background from 10 to 30° is from the Kapton film used to seal the XRD sample. The electron diffraction pattern in the inset is taken along the [003] zone axis, which is perpendicular to the *ab* TM plane. (b) XANES spectra at the Mn, Fe, Co, Ni K-edges of pristine MFCN and different transition metal oxide samples with standard valence states, including MnO (Mn^{2+}), Mn_2O_3 (Mn^{3+}), MnO_2 (Mn^{4+}), FeO (Fe^{2+}), Fe_2O_3 (Fe^{3+}), CoO (Co^{2+}), $LiCoO_2$ (Co^{3+}), $LiNi_{1/3}Co_{1/3}Mn_{1/3}O_2$ (Ni^{2+}), $LiNiO_2$ (Ni^{3+}), $Li_{0.2}Ni_{1/3}Co_{1/3}Mn_{1/3}O_2$ (Ni^{4+}).

which were simultaneously collected during each measurement. The X-ray absorption near edge structure (XANES) and extended X-ray absorption fine structure (EXAFS) spectra were processed using the Athena and Artemis software package [17,18].

The cathode film was made by mixing MFCN powder, Super P carbon black (Timcal) and dry PTFE (DuPont) with the weight ratio of 80:15:5. A Swagelok battery was assembled using glass fiber (Whatman GF/F) as a separator, Na metal (99.95% Sigma-Aldrich) as an anode and 1 M $NaPF_6$ (98%, Sigma-Aldrich) in EC:DEC (anhydrous, 1:1 volume ratio) as an electrolyte with the moisture level less than 3 ppm. The galvanostatic cycling was tested on Solartron 1470E at C/10 rate between 1.9–4.3 V on the cathode film with the loading of 2.2 mg/cm^2.

The in-situ lab XRD was taken on a Bruker D8 X-ray diffractometer equipped with a Mo source from a homemade in-situ electrochemical cell with Be window at MIT. The in-situ cell was charged galvanostatically at C/50 rate between 2.0 to 4.5 V on Solartron

Table 1
Mn, Fe, Co and Ni K-edge EXAFS structure parameters of pristine MFCN.

TM in MFCN	Path	r/Å	$\sigma^2/10^{-3}$ Å^2	ΔE/eV	R
Mn	Mn–O	1.92(8) ± 0.014	3.56 ± 1.72	−0.70 ± 2.53	0.003
	Mn–TM	2.94(7) ± 0.005	2.95 ± 1.03		
	Mn–Na	3.03(1) ± 0.122	17.65 ± 11.48		
Fe	Fe–O	2.01(1) ± 0.006	6.10 ± 10.70	0.12 ± 1.62	0.001
	Fe–TM	2.94(9) ± 0.004	3.89 ± 6.59		
	Fe–Na	3.21(1) ± 0.059	58.65 ± 42.42		
Co	Co–O	1.94(5) ± 0.010	4.18 ± 1.36	0.47 ± 1.97	0.002
	Co–TM	2.91(8) ± 0.009	4.62 ± 0.87		
	Co–Na	3.03(3) ± 0.046	40.30 ± 24.19		
Ni	Ni–O	2.05(4) ± 0.007	6.81 ± 1.23	−1.56 ± 0.88	0.001
	Ni–TM	2.94(9) ± 0.005	4.11 ± 0.70		
	Ni–Na	3.31(4) ± 0.036	13.24 ± 5.65		

r: bond length; σ^2: Debye–Waller factor (disorder); Δ*E*: inner shell potential shift; *R*: R-factor.

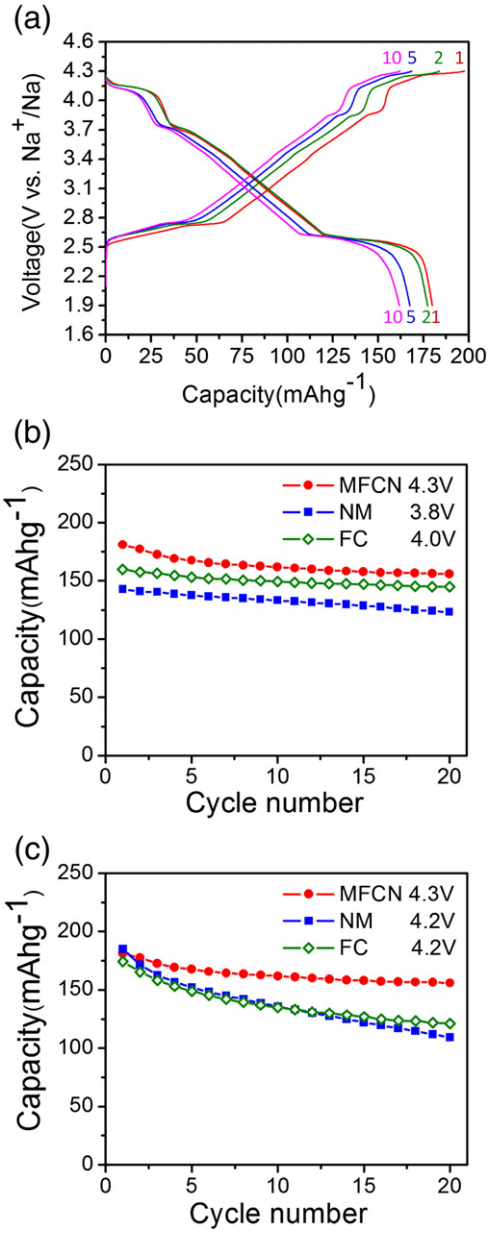

Fig. 2. (a) Galvanostatic charge and discharge profiles at 1st, 2nd, 5th and 10th cycles for MFCN. (b) Discharge capacity of MFCN cycled between 1.9–4.3 V at different cycles compared with NM cycled between 1.9–3.8 V and FC cycled between 1.9–4.0 V, all at C/10 rate. (c) Discharge capacity of MFCN cycled between 1.9–4.3 V at different cycles compared with NM and FC cycled between 1.9–4.2 V, all at C/10 rate.

1287 with each XRD pattern scanned from 6.5° to 30.5° 2θ (equivalent to 14.1° to 69.7° on Cu source) for 1 h, corresponding to 2% Na composition resolution per pattern. The phases in the in-situ XRD spectra were identified by Rietveld refinement.

3. Results and discussion

Fig. 1a shows that the XRD pattern is without any impurity peaks and the XRD refinement is fit well by using R-3m symmetry and assuming a random mixture of the TM ions in the TM layer. The refined structural parameters are shown in the inset of Fig. 1a. Table 1 shows the least-square fitting results from Fourier transformed (FT) EXAFS spectra on the Mn, Fe, Co, Ni K-edges of pristine MFCN. The interatomic distances from XRD refinement for TM–O, TM–TM and TM–Na ions are 2.009 Å, 2.954 Å and 3.153 Å, respectively, consistent with the values of 1.985 Å, 2.941 Å and 3.147 Å averaged from the bond lengths listed in Table 1. The electron diffraction pattern in the inset of Fig. 1a is taken perpendicular to the *ab* plane of pristine MFCN and shows no superstructure reflection, indicating no long range ordering for transition metal ions. These results are consistent with a solid solution of the four transition metal ions mixed in the TM layer of MFCN.

By comparing the edge positions in XANES (Fig. 1b) with standard samples of transition metal oxides the valence states of Mn, Fe, Co, Ni in pristine MFCN are determined as 4+, 3+, 3+, and 2+, respectively. The TM–O bond lengths of different TM ions in Table 1 also agree well with the ion radii of the TM ions with the valence states determined by XANES. The measured valence states of the four transition metal ions in MFCN are the same as in the NM and FC systems [11,16]. However, both the electrochemical performance and the structural evolution of MFCN show some significant differences from the two binary TM systems, indicating that MFCN is not a simple combination of NM and FC.

Fig. 2a shows the galvanostatic charge and discharge profiles of MFCN between 1.9 V–4.3 V at C/10 rate. The initial discharge capacity of 180 mAh/g occurs over an average discharge voltage of 3.21 V, making the specific energy density ≈578 Wh/kg. Fig. 2b shows the cycling performance of MFCN between 1.9 and 4.3 V compared with NM cycled between 1.9–3.8 V and FC cycled between 1.9–4.0 V, all at C/10 rate. MFCN shows a higher initial discharge capacity with comparable cyclability to NM and FC. Fig. 2c compares the cyclability of MFCN cycled between 1.9–4.3 V with NM and FC cycled between the same limits of 1.9–4.2 V, and at C/10 rate. Both NM and FC show much more significant capacity fading compared with MFCN. It has been speculated that the capacity fading of NM and FC cycled above 4.0 V is due to electrolyte decomposition [11,12,16]. However, the improved cycling performance of MFCN over NM and FC in the same type of electrolyte and high cutoff voltage range suggests that the different cycling performance between these compounds also has an intrinsic issue.

Fig. 3 shows the characteristic *hkl* peak evolution of the phases in MFCN in the first galvanostatic cycle between 2.0–4.5 V together with the in-situ charge and discharge profiles. The lattice parameter evolution calculated from the in-situ XRD measurement is also shown in Fig. 3. The (003) peaks of the O3 phase shift to lower angle and the (01–4) peaks to higher angle upon Na de-intercalation, corresponding to the typical expansion of the interplanar distance and decrease of the intra-planar distance. Two-phase coexistence of O3 and P3 occurs for 20–26% Na de-intercalation, followed by the transition to the P3 phase beyond 26% Na de-intercalation. The transition is characterized by a significant intensity decrease of the (01–4) peak of O3 and an increase of the (015) peak of P3. At 66% Na de-intercalation the P3 phase transforms to a new hexagonal O3 phase labeled as O3′ associated with a shift of the (003) peak back toward higher angle, corresponding to a decrease of the interplanar distance. Beyond 80% Na de-intercalation the (003) peak experiences large shifts to high angle forming another new hexagonal O3 phase labeled as O3″ with significant peak broadening, corresponding to highly decreased average inter-slab distances even below the value of the fully sodiated state. We suspect that stacking faults between the slabs cause the peak broadening. The phase transition processes are reversible upon discharge as shown in Fig. 3.

One feature of the structural evolution of MFCN is that no monoclinic distortion is observed during Na de-intercalation. This is very different from the NM system where multiple phase transitions between hexagonal and monoclinic phases are observed [12,16]. Monoclinic

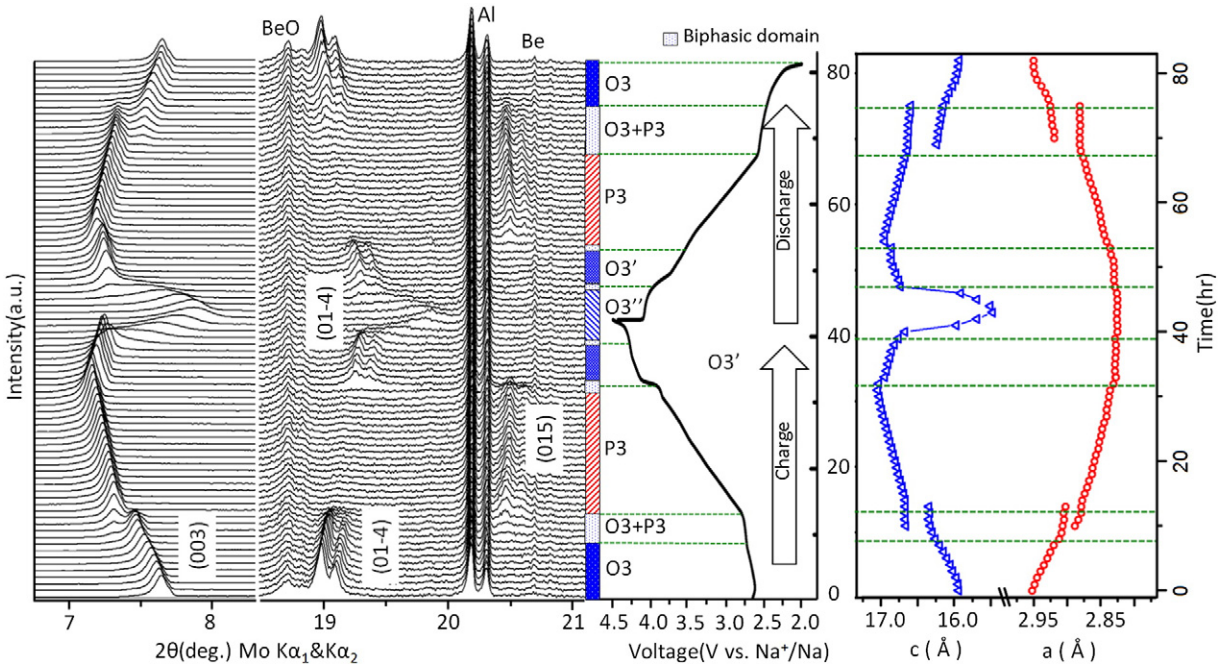

Fig. 3. In-situ lab XRD taken at 1 hour scanning rate per pattern shows the characteristic *hkl* peak evolution in different phases (left), corresponding to the in-situ galvanostatic charge and discharge profiles at C/50 rate (middle). The lattice parameter evolution (right) is calculated from in-situ XRD refinement. The double peaks in 01–4 and 015 peaks are from the $K\alpha_1$ and $K\alpha_2$ emissions in the Mo X-ray source.

distortions usually arise from anisotropic Na ordering such as the stripe ordering [19], Jahn–Teller distortion of the TM ions, or the coupling between them [19]. The absence of anisotropic Na ordering in MFCN may be a result of Na site disorder caused by the perturbations of the TM disorder. The particular TM composition in MFCN also reduces the amount of active Jahn–Teller ions, with only 25% Ni in the TM layer as compared with 50% in the NM system. These factors may largely suppress any monoclinicity, giving a much smoother electrochemical profile for MFCN compared with the more stepwise-like profile in the NM system.

Although FC shows excellent cycling performance when cycled below 4.0 V cutoff voltage [11], our result shows that the cyclability drops significantly when the cutoff voltage is increased to 4.2 V, which may indicate some structural instability and irreversibility of FC at high voltage and/or very low Na composition. On the contrary, our in-situ XRD of MFCN shows that the high voltage O3′ and O3" phases are reversible in the initial cycle, consistent with the reversible features observed in the first charge and discharge electrochemical profiles. However, we also notice that the O3" phase region of MFCN above 4.25 V is not fully reversible in the following cycles as observed in Fig. 2a. It is thus also important to understand the mechanism of capacity fading in the O3" phase of MFCN in future studies.

4. Conclusion

A new Na ion battery cathode material with composition $Na(Mn_{0.25}Fe_{0.25}Co_{0.25}Ni_{0.25})O_2$ is synthesized by the solid state reaction and shows an initial discharge capacity of 180 mAh/g and specific energy density of 578 Wh/kg. At high cutoff voltage the cycling performance of MFCN is noticeably better than that for the $Na(Fe_{0.5}Co_{0.5})O_2$ and $Na(Ni_{0.5}Mn_{0.5})O_2$, indicating a difference in the intrinsic properties of these compounds. The structural evolution in MFCN shows reversible phase transitions in the high voltage range and the absence of monoclinic distortions. The results show that MFCN is a high capacity cathode material and an important model system to investigate the general issue of capacity limits and fading of layered Na-TM cathodes for Na-ion batteries.

Conflict of interest

The authors declare that there is no conflict of interest.

Acknowledgments

This work was supported by the Samsung Advanced Institute of Technology. The XAS work at Brookhaven National Laboratory was supported by the U.S. Department of Energy, the Assistant Secretary for Energy Efficiency and Renewable Energy, Office of Vehicle Technologies under Contract No. DE-AC02-98CH10886.

References

[1] C. Delmas, C. Fouassier, P. Hagenmuller, Structural classification and properties of the layered oxides, Phys. B + C 99B (1980) 81–85 (http://www.sciencedirect.com/science/article/pii/0378436380902144 (accessed November 10, 2013)).
[2] C. Delmas, J. Braconnier, C. Fouassier, P. Hagenmuller, Electrochemical intercalation of sodium in Na_xCoO_2 bronzes, Solid State Ionics 4 (1981) 165–169.
[3] C. Didier, M. Guignard, C. Denage, O. Szajwaj, S. Ito, I. Saadoune, et al., Electrochemical Na-deintercalation from $NaVO_2$, Electrochem. Solid-State Lett. 14 (2011) A75, http://dx.doi.org/10.1149/1.3555102.
[4] X. Ma, H. Chen, G. Ceder, Electrochemical properties of monoclinic $NaMnO_2$, J. Electrochem. Soc. 158 (2011) A1307, http://dx.doi.org/10.1149/2.035112jes.
[5] P. Vassilaras, X. Ma, X. Li, G. Ceder, Electrochemical properties of monoclinic $NaNiO_2$, J. Electrochem. Soc. 160 (2012) A207–A211, http://dx.doi.org/10.1149/2.023302jes.
[6] S. Komaba, C. Takei, T. Nakayama, A. Ogata, N. Yabuuchi, Electrochemical intercalation activity of layered $NaCrO_2$ vs. $LiCrO_2$, Electrochem. Commun. 12 (2010) 355–358.
[7] N. Yabuuchi, H. Yoshida, S. Komaba, Crystal structures and electrode performance of alpha-$NaFeO_2$ for rechargeable sodium batteries, Electrochemistry 80 (2012) 716 (http://jlc.jst.go.jp/DN/JST.JSTAGE/electrochemistry/80.716?from=Google (accessed August 09, 2014)).
[8] S.P. Ong, V.L. Chevrier, G. Hautier, A. Jain, C. Moore, S. Kim, et al., Voltage, stability and diffusion barrier differences between sodium-ion and lithium-ion intercalation materials, Energy Environ. Sci. 4 (2011) 3680, http://dx.doi.org/10.1039/c1ee01782a.
[9] X. Wang, G. Liu, T. Iwao, Role of ligand-to-metal charge transfer in O3-type $NaFeO_2$–$NaNiO_2$ solid solution for enhanced electrochemical properties, J. Phys. (2014) 2–8 (http://pubs.acs.org/doi/abs/10.1021/jp411382r (accessed September 23, 2014)).
[10] I. Saadoune, A. Maazaz, M. Menetrier, C. Delmas, On the $Na_xNi_{0.6}Co_{0.4}O_2$ system: physical and electrochemical studies, J. Solid State Chem. 117 (1996) 111–117.
[11] H. Yoshida, N. Yabuuchi, S. Komaba, $NaFe_{0.5}Co_{0.5}O_2$ as high energy and power positive electrode for Na-ion batteries, Electrochem. Commun. 34 (2013) 60–63.
[12] S. Komaba, T. Nakayama, A. Ogata, T. Shimizu, C. Takei, S. Takada, et al., Electrochemically reversible sodium intercalation of layered $NaNi_{0.5}Mn_{0.5}O_2$ and $NaCrO_2$, ECS Trans. 16 (2009) 43–55.
[13] D. Kim, E. Lee, M. Slater, W. Lu, S. Rood, C.S. Johnson, Layered $Na[Ni_{1/3}Fe_{1/3}Mn_{1/3}]O_2$ cathodes for Na-ion battery application, Electrochem. Commun. 18 (2012) 66–69, http://dx.doi.org/10.1016/j.elecom.2012.02.020.
[14] M. Sathiya, K. Hemalatha, K. Ramesha, J.-M. Tarascon, A.S. Prakash, Synthesis, structure, and electrochemical properties of the layered sodium insertion cathode material: $NaNi_{1/3}Mn_{1/3}Co_{1/3}O_2$, Chem. Mater. 24 (2012) 1846–1853.
[15] P. Vassilaras, A.J. Toumar, G. Ceder, Electrochemical properties of $NaNi_{1/3}Co_{1/3}Fe_{1/3}O_2$ as a cathode material for Na-ion batteries, Electrochem. Commun. 38 (2014) 79–81, http://dx.doi.org/10.1016/j.elecom.2013.11.015.
[16] S. Komaba, N. Yabuuchi, T. Nakayama, A. Ogata, T. Ishikawa, I. Nakai, Study on the reversible electrode reaction of $Na1 - xNi_{0.5}Mn_{0.5}O_2$ for a rechargeable sodium-ion battery, Inorg. Chem. 51 (2012) 6211–6220 (http://pubs.acs.org/doi/abs/10.1021/ic300357d (accessed August 10, 2014)).
[17] M. Newville, IFEFFIT: interactive XAFS analysis and FEFF fitting, J. Synchrotron Radiat. 8 (2001) 322–324 (http://scripts.iucr.org/cgi-bin/paper?ph5149 (accessed August 11, 2014)).
[18] B. Ravel, M. Newville, ATHENA, ARTEMIS, HEPHAESTUS: data analysis for X-ray absorption spectroscopy using IFEFFIT, J. Synchrotron Radiat. 12 (2005) 537–541, http://dx.doi.org/10.1107/S0909049505012719.
[19] X. Li, X. Ma, D. Su, L. Liu, R. Chisnell, S. Ong, et al., Direct visualization of the Jahn–Teller effect coupled to Na ordering in $Na_5/8MnO_2$, Nat. Mater. 13 (2014) 586–592, http://dx.doi.org/10.1038/NMAT3964.